Frequency-Domain Photoacoustic Phase Spectroscopy: A Fluence-Independent Approach for Quantitative Probing of Hemoglobin Oxygen Saturation

Bahman Lashkari, Sung soo Sean Choi, Edem Dovlo, Saheb Dhody, and Andreas Mandelis

***Abstract*—In this paper, it is shown that the phase of the frequency-domain photoacoustic (PA) signal can be used to measure the absorption coefficient (μ_a) of the chromophore. This method can be referred to as a calibration-free approach in the sense that it is not affected by the attenuation of fluence in the tissue. This helps to enhance the accuracy of quantitative PA functional imaging. However, the premise for employing the aforementioned method is that chromophore geometry should be known *a priori*. As a proof of applicability of the theory, the method was applied to a simplified geometry and the extension of the method to more complicated geometries is discussed. One of the key subjects of functional imaging in medicine is blood. Parameters such as total hemoglobin concentration and hemoglobin oxygen saturation are valuable for diagnostics as well as for treatment of many diseases. The developed method was employed for *in vitro* monitoring of blood oxygenation on heparinized sheep blood and is applicable to characterization problems in biological tissues and other turbid media.**

***Index Terms*—Biomedical optical imaging, frequency modulation, photoacoustic effects, spectroscopy.**

I. Introduction

BIOMEDICAL photoacoustic (PA) imaging can roughly be described as a mapping method based on the optical absorption properties of tissue. The tissue specific absorption of monochromatic light is the source of exceptional contrast and spectroscopic capability of PA. Unquestionably, the ability of functional imaging has been among the leading advantages of PA [1], [2]. Knowing the absorption coefficient of different components, for instance, oxyhemoglobin and deoxyhemoglobin at specific wavelengths, enables the extraction of a concentration map of these components from PA measurements. Thus, PA spectroscopy has a great clinical advantage in providing a noninvasive method for monitoring the symptoms and biological functionalities without the depth limitations of similar purely optical spectroscopic techniques. This capability has been widely investigated by acquiring multiple wavelength signals from the chromophore [3], [4]. The preclinical and clinical applications are broad; examples are functional imaging of small animals [4], [5], detecting human cancerous tumors [6], [7], and imaging lipid-rich plaques in the myocardial artery [8].

The existence of commercial instruments that provide this capability may suggest that the technology is quite mature [9], [10]. However, the method has several restrictions; the first problem is that the laser fluence is assumed to be known in tissue. For instance, optical scattering may be assumed to be wavelength-independent. To comply with this assumption sometimes the wavelengths used are chosen to be very close. Moreover, the fluence is assumed to be uniform in the part of the object under investigation. In reality, since the fluence is unknown in a given situation, this method can only provide a qualitative absorption distribution and not absolute values. Another source of error is the variation in the physical properties of different tissues as well as those of the various organs. For instance, the Grüneisen coefficients of blood and lipids are considerably different [11]–[13], although, due to their distinct optical spectra, the differences may not be easy to evaluate. Further limitations and conventional assumptions of quantitative PA imaging are discussed elsewhere [12]–[14]. In conclusion, one should be aware of all the very restrictive assumptions required to consider a PA image as a map of absorption coefficient: One should be aware that "PA images are not images of the absorption coefficient" [12].

The published theoretical work in PA signal generation reveals that the shape of the PA signal is also affected by the absorption coefficient [15], [16]. This property offers another opportunity to characterize a chromophore independently of the fluence. Based on this approach, a methodology has been suggested that can measure the absorption and scattering properties of *in-vitro* tissue [17]. Consideration of the transient shape of the PA signal has also been given toward the clinical quantification of cerebral blood oxygenation via monitoring the superior sagittal sinus or the jugular vein [18]–[20]. This attempt was based on a one-dimensional (1-D) solution of pulsed PA to obtain the absolute absorption coefficient by measuring the risetime of the PA signal [18]. The method, however, faces the challenges related to 1-D solution approximation and the requirement for an ultra-wideband detector. On the other hand, the advantage of this method is that it is independent of fluence variation with wavelength in tissues. Another advantage is that it requires only one wavelength to extract the absorption coefficient [18]. In subsequent studies aimed at increasing the accuracy of oxygenation

Manuscript received August 5, 2015; revised October 7, 2015; accepted October 20, 2015. Date of publication October 26, 2015; date of current version February 18, 2016. This work was supported by the Natural Sciences and Engineering Research Council of Canada under a Discovery Grant and by CIHR-NSERC CHRP Grant.

The authors are with the Center for Advanced Diffusion-Wave Technologies, Department of Mechanical and Industrial Engineering, University of Toronto, Toronto, ON M5S 3G8, Canada (e-mail: bahman@mie.utoronto.ca; sungsujaing@hotmail.com; edovlo@mie.utoronto.ca; saheb.dhody@mail.utoronto.ca; mandelis@mie.utoronto.ca).

Color versions of one or more of the figures in this paper are available online at http://ieeexplore.ieee.org.

Digital Object Identifier 10.1109/JSTQE.2015.2494532

estimates, the researchers employed at least three wavelengths, one around the isosbestic point (800 nm), one above (1064 nm), and one below that point (680 or 700 nm) [19], [20]. This application was also examined *in-vivo* using the conventional amplitude method by calibrating the optical attenuation obtained from a phantom study with the abovementioned three wavelengths [21], [22].

Another approach to obtain oxygen saturation and total hemoglobin concentration without the requirement for the measurement or estimation of optical attenuation is through the acquisition of the acoustic spectra of the PA signal. Dividing the acoustic spectrum at one wavelength (only absolute amplitude) by that at another wavelength, automatically eliminates the acoustic attenuation and the system transfer function [23], [24]. This method was labeled "calibration-free" by the authors as it does not require any adjustment on the detected signals to compensate for optical attenuation. Similarly, the ratios of amplitudes of the PA signal at a fixed wavelength and different oxygen saturation (SO_2) levels were employed, which eliminates fluence from each wavelength [25]. This method tends to provide amplitude ratios, therefore, it requires two wavelengths for oxygen saturation estimation (constant total hemoglobin concentration, tHb) and three wavelengths for estimation of both total hemoglobin concentration and oxygen saturation.

A fundamental approach to the PA tissue characterization problem is to provide a numerical simulation of the PA response in parallel with the experiments. The numerical simulations can consider both scattering and absorption properties of the target chromophore and numerically simulate light penetration in the tissue, followed by a model-based inversion of the PA signals. This solution requires complicated and time consuming numerical calculations. Different models of light diffusion in tissue are employed and the numerical methods are iteratively corrected with the experimental data [11], [13], [26]. The goal of those methodologies is to reach an accurate quantitative map of concentration/distribution of dominant absorbers in the PA interrogated tissue.

Another attempt to obtain the absolute absorption coefficient of chromophores from detected PA signals employed the iterative numerical solution of the exact PA wave equation considering the temporal excitation laser profile. The error between the detected and simulated peak-to-peak ratio of the PA signal was used as the criterion to iteratively converge the numerical solution [27].

Similar to the main trend of pulsed PA functional imaging, the amplitude of frequency-domain (FD) PA signal is proportional to the absorption coefficient and thus, it facilitates functional imaging [28]. This method has been used for estimations of blood oxygen saturation level *in-vitro* and *in-vivo* [29]. Furthermore, the potential for the manipulation of phase, amplitude and frequency provides important quantitative measurement opportunities in FD. For instance, it has been shown that it is possible to perform simultaneous imaging with multiple wavelengths by using mismatched coded excitations [29] or greatly enhance signal dynamic range and sensitivity by performing differential wavelength-modulated probing [30], [31]. Nevertheless, these FD methods do not provide any advantage or disadvantage with regard to errors caused by wavelength-dependent fluence

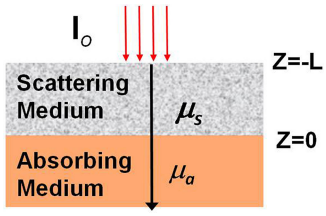

Fig. 1. Simple 1-D model of PA signal generation.

distribution in the tissue. In this work, we use another feature of FD-PA within the framework of a 1-D solution, whereby it is demonstrated that the phase value in FD-PA contains valuable information about the absorption coefficient, the measurement of which is not affected by fluence attenuation or variations. Thus, the analysis of the phase of the cross-correlation (CC) signal in the vicinity of the CC peak can be related to the absorption coefficient without the requirement for the estimation of laser light fluence. It is demonstrated that only one wavelength is required to obtain the absolute absorption coefficient of a target chromophore, a procedure which requires a theoretical fitting-based approach. For more practical application of SO_2 estimates, two wavelengths were employed. For variable tHb, the suggested method requires three wavelengths to obtain both unknowns.

II. Theoretical Background

The goal of this section is to demonstrate that the phase of the PA CC signal can provide quantitative absorption coefficient information of subsurface laser-stimulated chromophores. We start from the 1-D solution of the back-propagating PA signal generated by a large uniform laser beam from a flat semi-infinite absorber located below a scattering medium (see Fig. 1). In the Fourier domain [32]:

$$\tilde{p}_s(-L,f) = \frac{\Gamma\, e^{-\mu_{eff}L}}{\left(1+\frac{\rho_a c_a}{\rho_s c_s}\right)} \frac{\mu_a}{\mu_a c_a + j\omega} e^{-jk_s L}\tilde{I}_o(f) \quad (1)$$

where the tilde indicates the Fourier transform operation; $k_s = \omega/c_s$ is the acoustic angular wavenumber; ω is the angular frequency, $\omega = 2\pi f$; $c_a(c_s)$ is the speed of sound in the absorbing (scattering) medium; ρ_a (ρ_s) is the density of the absorbing (scattering) medium; μ_a is the absorption coefficient of the absorbing medium; Γ is the efficiency of thermo-acoustic excitation (Grüneisen coefficient); μ_{eff} is the effective optical attenuation coefficient of the scattering medium; L is the thickness of the scattering overlayer medium (the distance of the transducer from the absorber surface); I_o is the laser intensity on the surface. The ratio $\rho_a c_a/(\rho_s c_s)$ is normally set to one. For most soft tissue cases, this approximation is appropriate, however, in some special cases such as where one medium is hard tissue, this ratio affects the PA signal [33].

One prevalent excitation waveform in FD PA is a linear frequency modulation (LFM) chirp leading to PA radar operation

and described by

$$I_o(t) = A_I \left[1 + \sin\left(2\pi f_c t + \frac{\pi B_{ch}}{T_{ch}} t^2\right)\right], \; -\frac{T_{ch}}{2} < t < \frac{T_{ch}}{2}, \tag{2}$$

where A_I is the average power; f_c, T_{ch} and B_{ch} are the center angular frequency, duration and frequency bandwidth of the chirp, respectively.

Based on (1), the CC signal for a LFM chirp was shown to be [32]:

$$R(t) \approx \left(\frac{2\Gamma\, \mu_a e^{-\mu_{eff} L}}{1 + \frac{\rho_a c_a}{\rho_s c_s}} \left(A_I \frac{T_{ch}}{4B_{ch}}\right)\right) \times \left[\int_{f_c - \frac{B_{ch}}{2}}^{f_c + \frac{B_{ch}}{2}} \left(\frac{e^{-\alpha_s f L}}{\mu_a c_a + j\omega}\right) e^{j\omega\left(t - \frac{L}{c_s}\right)} \tilde{H}_{tr}(f)\, df\right] \tag{3}$$

where H_{tr} is the transfer function of the ultrasonic transducer; α_s is the acoustic attenuation coefficient. The real and imaginary parts of *R*(*t*) correspond to the in-phase and quadrature CC signals, respectively; therefore, the phase of the CC signal is defined as:

$$\theta(t) = \tan^{-1}\left\{\frac{\int_{f_c - B_{ch}/2}^{f_c + B_{ch}/2} \left[\left(\frac{\mu_a c_a - j\omega}{(\mu_a c_a)^2 + \omega^2}\right) e^{j\omega\left(t - \frac{L}{c_s}\right)} \tilde{H}_{tr}(f) e^{-\alpha_s f L}\right]_{imag.} df}{\int_{f_c - B_{ch}/2}^{f_c + B_{ch}/2} \left[\left(\frac{\mu_a c_a - j\omega}{(\mu_a c_a)^2 + \omega^2}\right) e^{j\omega\left(t - \frac{L}{c_s}\right)} \tilde{H}_{tr}(f) e^{-\alpha_s f L}\right]_{real} df}\right\}. \tag{4}$$

The four multiplicative terms in the bracket are the PA response (1-D solution), delay term, transducer transfer function, and acoustic attenuation, respectively. It can be seen that the phase of the CC signal is independent of fluence ($A_I e^{-\mu_{eff} L}$) and Grüneisen coefficient (Γ). For an ideal case where the transducer spectrum behaves as a top hat bandpass filter, and acoustic attenuation is insignificant, their corresponding terms can be cancelled. Then, under the condition of very large bandwidth, the delay term at the negative peak of the quadrature CC is simply equal to 1 (i.e., at $t = L/c_s$) [32].

PA detection mostly uses the near-IR imaging window where absorption is quite low. Therefore, selecting a chirp frequency range which satisfies $(\mu_a c_a)^2 << \omega^2$, the above equation can be simplified and the integrals can readily be evaluated at $t = L/c_s$. The result is

$$\theta\left(t = \frac{L}{c_s}\right) \approx \tan^{-1}\left\{\frac{1}{\mu_a c_a} \frac{\int_{f_c - B_{ch}/2}^{f_c + B_{ch}/2} \left(\frac{-df}{\omega}\right)}{\int_{f_c - B_{ch}/2}^{f_c + B_{ch}/2} \left(\frac{df}{\omega^2}\right)}\right\} = \tan^{-1}\left\{\frac{2\pi\left(f_c^2 - B_{ch}^2/4\right) \ln\left(\frac{f_c - B_{ch}/2}{f_c + B_{ch}/2}\right)}{\mu_a c_a B_{ch}}\right\}. \tag{5}$$

Equation (5) theoretically shows that the phase of the CC signal at delay time $t = L/c_s$ can readily yield the absorption coefficient of the chromophore in an analytical form:

$$\mu_a \approx \frac{2\pi\left(f_c^2 - B_{ch}^2/4\right) \ln\left(\frac{f_c - B_{ch}/2}{f_c + B_{ch}/2}\right)}{c_a B_{ch} \tan\left[\theta(t = L/c_s)\right]}. \tag{6}$$

This method can obtain the absolute absorption coefficient using only one wavelength. This simplified equation can be very helpful if one wants to use a bench-top instrument similar to the one described elsewhere based on the pulsed PA temporal profile [17]. The prerequisite for using (6) is to be able to accurately measure the distance *L* to the chromophore.

Even in the case where the 1-D solution is valid, there are two practical challenges facing the use of (6) for quantitative PA imaging. First, the peak of the quadrature PA CC signal does not exactly correspond to $t = L/c_s$. The limited bandwidth of the detector, frequency dependent acoustic attenuation and transducer transfer function shift the peak slightly (by a few tens of nanoseconds). The second challenge is the complex transfer function of the transducer (or the whole measurement system) that affects the CC signal and thus, its phase.

The transfer function of the transducer and other parts of the instrumentation can be obtained empirically. Then a Wiener filter can be employed to deconvolve the PA signal from the transfer function. By multiplying the CC spectrum by $\frac{\tilde{H}_{tr}^*(f)}{\tilde{H}_{tr}(f)\tilde{H}_{tr}^*(f) + N(f)/S(f)}$, the effect of the transducer will be eliminated:

$$R_{\text{estimate}}(f) = \frac{\tilde{H}_{tr}^*(f)}{\tilde{H}_{tr}(f)\,\tilde{H}_{tr}^*(f) + 1/\text{SNR}(f)} R_{meas}(f). \tag{7}$$

Here *N* and *S* are the power spectra of the noise and the actual signal, respectively.

In order to be able to employ Wiener deconvolution, the SNR(*f*) is approximated by the ratio of the measured CC power spectrum over the standard deviation of the power spectrum in several measurements. Thus, the second challenge, the effect of transducer transfer function, can be resolved. Therefore, if the delay time corresponding to L/c_s can be determined, the method is applicable to extract μ_a. Recalling (4), a new time-shifted parameter $\tau = t - L/c_s$ can be defined. The exact delay time is known to be very close to the signal peak and therefore an asymptotic solution of the phase value can be found for small values of τ. Again ignoring the transducer effect and attenuation, we obtain:

$$\theta(\tau) \approx \tan^{-1}\left\{\frac{\int_{f_c - B_{ch}/2}^{f_c + B_{ch}/2} \left[\left(\frac{\mu_a c_a - j\omega}{\omega^2}\right)(\cos\omega\tau + j\sin\omega\tau)\right]_{imag.} df}{\int_{f_c - B_{ch}/2}^{f_c + B_{ch}/2} \left[\left(\frac{\mu_a c_a - j\omega}{\omega^2}\right)(\cos\omega\tau + j\sin\omega\tau)\right]_{real} df}\right\} \tag{8}$$

so that for $\omega\tau << 1$:

$$\theta(\tau) \approx \tan^{-1}\left\{\frac{\int_{f_c - B_{ch}/2}^{f_c + B_{ch}/2} \left[\left(\frac{\mu_a c_a - j\omega}{\omega^2}\right)(1 + j\omega\tau)\right]_{imag.} df}{\int_{f_c - B_{ch}/2}^{f_c + B_{ch}/2} \left[\left(\frac{\mu_a c_a - j\omega}{\omega^2}\right)(1 + j\omega\tau)\right]_{real} df}\right\} \approx \tan^{-1}\left\{\frac{(1 - \mu_a c_a \tau)\ln\left(\frac{f_c - B_{ch}/2}{f_c + B_{ch}/2}\right)}{\left(\frac{\mu_a c_a}{2\pi\left(f_c^2 - B_{ch}^2/4\right)} - 2\pi\tau\right) B_{ch}}\right\}. \tag{9}$$

To further simplify (9), the range of the parameters should be known a priori. For example, the absorption coefficient of oxy- and deoxy-hemoglobin at the employed wavelengths can be readily obtained from the literature [34]–[36]. Therefore, we can assume that a typical μ_a is in the range of 1–10 cm^{-1}. Also, speed of sound in soft tissue (c_s) is ca. 1500 m/s. The value of τ corresponding to the signal peak can be calculated by maximizing the denominators in (8). In typical PA imaging systems τ is in the range of tens of nanoseconds and the bandwidth (B_{ch}) is in the range of a few megahertz. Therefore, $1 - \mu_a c_a \tau \approx 1$. Both terms in the denominator are very small, thus, θ is approximately $\pm\pi/2$. Equation (8) can be simplified by using the first two terms of the Taylor series expansion for $\tan^{-1}$:

$$\theta(\tau) \approx \pm\frac{\pi}{2} - \frac{B_{ch}}{\ln\left(\frac{f_c - B_{ch}/2}{f_c + B_{ch}/2}\right)}\left(\frac{\mu_a c_a}{2\pi\left(f_c^2 - B_{ch}^2/4\right)} - 2\pi\tau\right) + \cdots. \tag{10}$$

This expression shows that the phase angle behaves asymptotically linearly near $\tau = 0$ (with a π jump). Since the exact value of L, and consequently τ, is unknown, it is possible to use a fitting-based method to find the closest μ_a value. In this work, for the proof of concept experiments on PVC-plastisol phantoms a fitting method was used to extract the absorption coefficients. However, the alternative approach is to use multiple wavelengths. Since the variation of phase around the peak is linear with very close slopes for different absorption coefficients, one can use the difference in the phase to measure the variation of absorption coefficient without the need to have the exact delay time. Using two wavelengths and subtracting the phase of the detected signals, (10) yields:

$$\theta_{\lambda_1}(\tau) - \theta_{\lambda_2}(\tau) \approx \frac{B_{ch}\ c_a}{2\pi\left(f_c^2 - B_{ch}^2/4\right)\ln\left(\frac{f_c + B_{ch}/2}{f_c - B_{ch}/2}\right)} \times(\mu_{a1} - \mu_{a2}) + \cdots. \tag{11}$$

This equation shows that the difference in the two PA phases induced by two different wavelengths is proportional to the difference in the absorption coefficient. The application of this method avoids the requirement for determining the exact delay time $t = L/c_s$. However, it requires an extra wavelength and additionally, knowledge of μ_a is only relative; one only knows $\Delta\mu_a$. For instance, for blood oxygenation characterization, it requires two wavelengths to estimate the oxygen saturation and three wavelengths to estimate both oxygen saturation and total hemoglobin concentration. The errors encountered in the evaluation of μ_a by using (6), (10) and (11) are shown in two sets of experiments discussed below.

III. Experimental Set-up

The experimental set-up is described elsewhere [29], [31]. The set-up consisted of two CW lasers; an 805 nm diode (Laser Light Solutions, NJ, USA) and a 680 nm diode laser (LDX Optronics, Inc., Maryville, TN, USA). The former was equipped with its own driver while the latter was modulated by a high-frequency driver VFM5-25 (MESSTEC, Germany). A dual-channel arbitrary waveform generator (33500B, Agilent Technologies, Inc., Loveland, CO, USA) was used to control the drivers. Both channels of the waveform generator were synchronized with a trigger from a National Instruments card. The signal generation and acquisition were controlled by an in-house LabView program. The output fibers of the two diode lasers were connected to two identical 0.8-mm collimators (F230SMA-B, Thorlabs, NJ, USA) which were directed toward the same point on the surface of the target. A focused ultrasonic transducer with 2.2-MHz center frequency V305 (Olympus NDT, Inc., Panametrics, USA) was placed in front of the measurement unit at around its focal distance (1 in). The output signal of the transducer was amplified by 40 dB (preamplifier 5676, Panametrics, Olympus, USA) before being digitized by a data acquisition card (NI PXIe-5122, TX, USA). Parts of the experiments were performed on a blood circulating rig, where a peristaltic pump (Pd5201, Heidolph Instruments GmbH & Co., Bavaria, Germany) was used to circulate sheep blood continuously flowing from a sealed blood bag to a flow cell (CFCAS0004, IBI Scientific, Peosta, IA, USA) and back to the blood bag through a plastic tubing (see Fig. 2(a)). For the plastisol experiments, phantoms were attached to a holder and placed at the focal distance in front of the transducer.

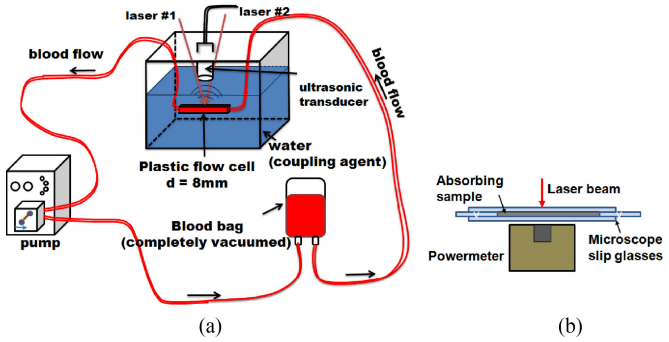

Fig. 2. (a) Experimental set-up. (b) Measurement of absorption coefficient of samples by a purely optical method.

IV. Single Wavelength Experiment on Homogeneous Semi-Infinite Plastisol Phantom

One experiment was performed on four PVC-plastisol samples with different absorption coefficients [37]. The goal of this experiment was to show that the phase of the PA CC signal is capable of yielding quantitative absorption coefficient measurements. The surfaces of the phantoms were flat and wide, so by using a large laser beam (>8 mm) they could be considered as a laterally semi-infinite geometry. In addition to PA measurements, the absorption coefficients of the phantoms were also measured through purely optical transmissions. During the production of each phantom, an extra thin layer sample of 1.1 ± 0.05 mm was also made. These thin-layer samples were produced by sandwiching the plastisol solution between two microscope slip glasses, with distance between the two glasses being controlled by another two similar glasses at both ends (see Fig. 2(b)). After solidification of these thin layers, their optical transmittances were measured. Optical scattering from these samples was negligible. The transmitted laser power was

TABLE I
THE MEASURED ABSORPTION COEFFICIENT OF PVC-PLASTISOL SAMPLES USING PURELY OPTICAL TRANSMISSIONS, AND PA AMPLITUDE AND PHASE

	Absorption coefficient estimates		
Sample	Optical method [cm^{-1}]	PA amplitude [cm^{-1}]	PA phase [cm^{-1}]
#1	**1.52 ± 0.15**	1.52*	1.52*
#2	**3.32 ± 0.19**	**3.19**	**3.32**
#3	**7.28 ± 0.37**	**6.54**	**7.01**
#4	**10.87 ± 0.56**	**9.50**	**10.69**

*The first sample was used to calibrate the PA measurements.

measured with and without the absorbing layer, which yielded the absorption coefficient. The measured absorption coefficients of the four samples are reported in Table I. The errors were estimated based on inaccuracy in the size of the samples as well as deviation of the powermeter readings during consecutive measurements.

The PA signals from the four plastisol samples were also detected in the foregoing experimental set-up. The 805 nm laser was employed with a linear intensity modulation in the 300 kHz to 2.5 MHz range. The duration of the transmitted chirp was 1 ms and signal detection was performed 200 times to provide the averaged detected signal for each phantom. Fig. 3(a) and (b) shows the detected in-phase CC signal and the envelope signal, respectively. The CC amplitudes grow with increasing relative absorption coefficient of the samples, as expected.

One of the absorbers can be used for system calibration purposes to estimate the absorption coefficients of other samples. The μ_a (at 805 nm) of the first sample is considered to be known (from the optical measurement) and those of other samples were calculated (linearly scaled) and reported in Table I. This experiment only employed one wavelength, therefore, intensity normalization for different wavelengths was not required.

To show that the PA CC phase can yield accurate absolute μ_a values, we used a fitting method to extract the absorption coefficients from the PA CC signals. Similar to the above, one absorber was used for system calibration. The detected signal from the first phantom was used to yield the transfer function of the system. Considering its known μ_a, the average spectrum of this signal as well as its standard deviation was used to determine the Weiner filter. The Weiner filter was applied to deconvolve all CC signals. The in-phase and quadrature CC signals after deconvolution are shown in Fig. 4. Equation (6) can be used to yield μ_a, where phase should be determined at $\tau = 0$. We assume that the point $t = L/c_s$ ($\tau = 0$) is very close to the signal peak (at t_p), that is, $t_p - L/c_s$ is very small. Therefore, for each sample, the root-mean-square (RMS) error of the predicted signal and deconvolved measured signal (see Fig. 4) versus $t - t_p$ values were calculated. $t - t_p$ was assumed to be in the range of -10 to 60 ns. The phase value was determined at each $t - t_p$ from the deconvolved signal. Then, (6) was used to calculate μ_a. When the calculated μ_a were negative, evidently the employed delay time was not the correct value; whenever positive, the evaluated μ_a was used to generate a theoretical PA signal. The RMS error of theoretical PA CC and deconvolved measured CC (see Fig. 4) was then calculated. The normalized error versus $t - t_p$ for phantom #2 is shown in Fig. 5. For all

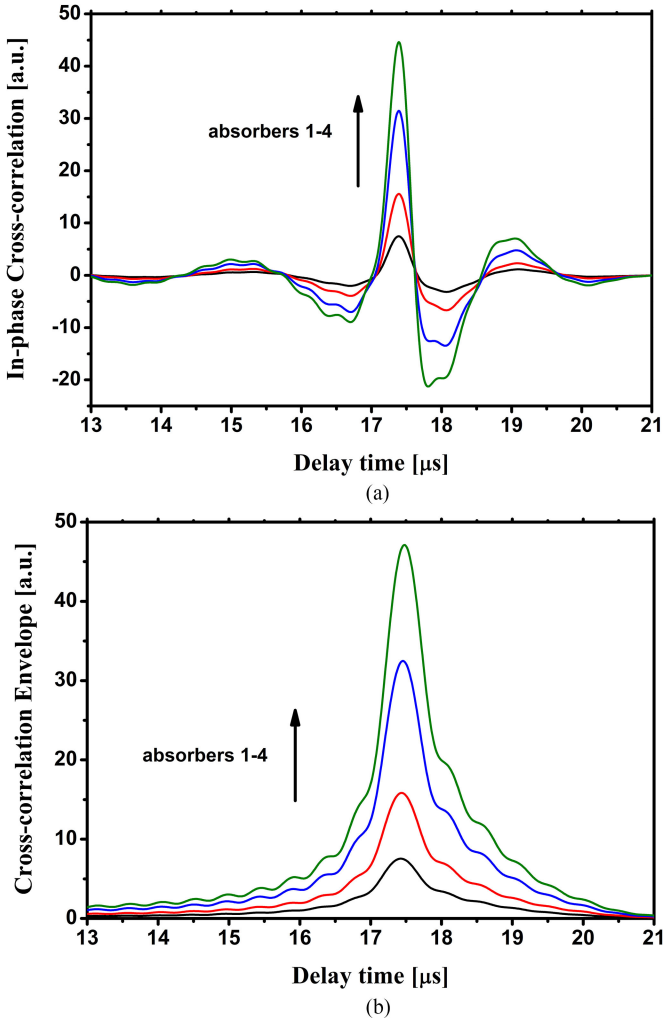

Fig. 3. (a) Detected in-phase PA CC and (b) CC envelope signals.

samples, the minimum RMS error was used to estimate $t - t_p$ and its corresponding μ_a. The estimated μ_a values for all samples are reported in Table I, where they are compared with the values determined from purely optical transmission and from PA amplitudes. The calculated phases near the peak of the PA signals are also depicted in Fig. 6, where the delay time $t = L/c_s$ is used to evaluate the absorption coefficients. Fig. 6 shows that the phase of the CC varies linearly around the peak and the variation in the slopes of phases versus μ_a is very small. In other words, the linear approximation presented in (10) is reasonably accurate. The application of the fitting-based method to determine μ_a is not very complicated for the simple case of one absorber (only one signal) but it can be complicated when signals from different layers are very close to each other.

V. DUAL-WAVELENGTH EXPERIMENTS ON *In-Vitro* CIRCULATING SHEEP BLOOD

Determination of hemoglobin oxygen saturation is among the most promising applications of PA, due to its clinical impact, noninvasiveness and application ease. The well tabulated and distinct absorption coefficients of oxy- and deoxy-hemoglobin

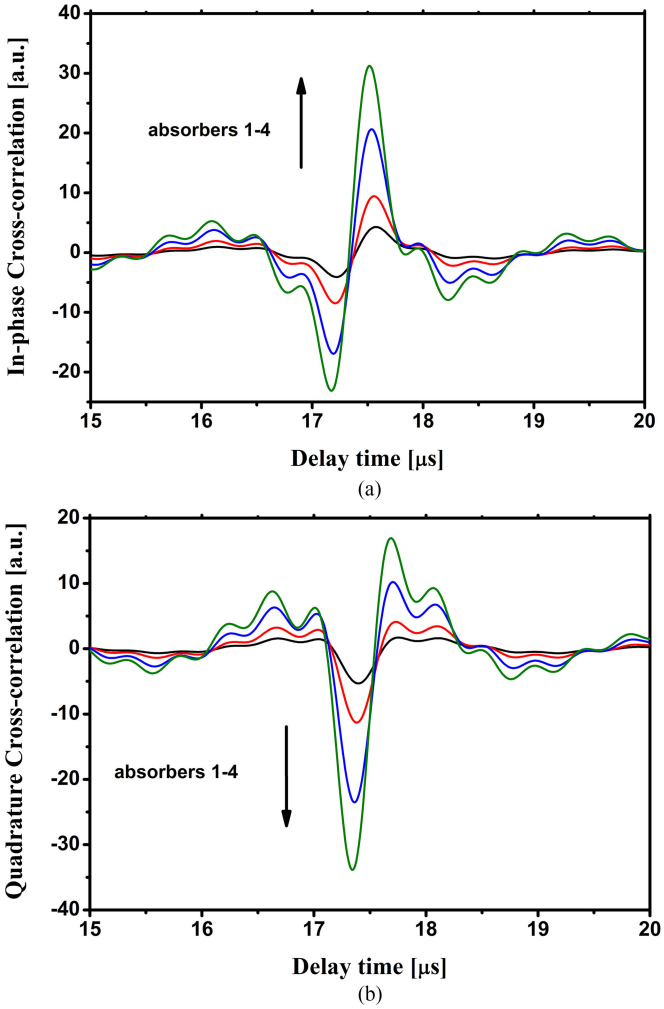

Fig. 4. (a) In-phase and (b) quadrature CC signals deconvoluted by Wiener filtering.

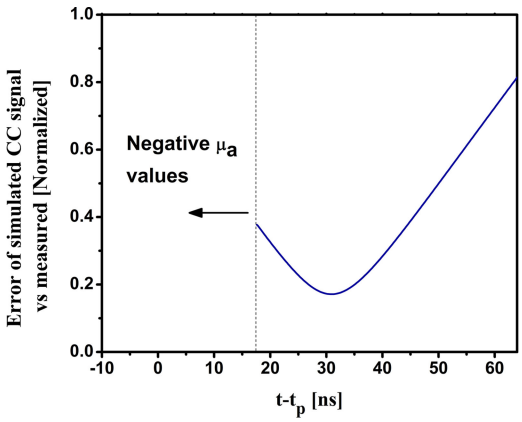

Fig. 5. The error in estimation of the signal profile with delay time $(t - t_p)$ variation.

facilitate the use of two or more wavelengths to determine this important parameter. In this experiment, we compared the use of the PA amplitude and PA phase in finding the hemoglobin oxygenation level. The *in-vitro* blood circulation set-up of Fig. 2(a)

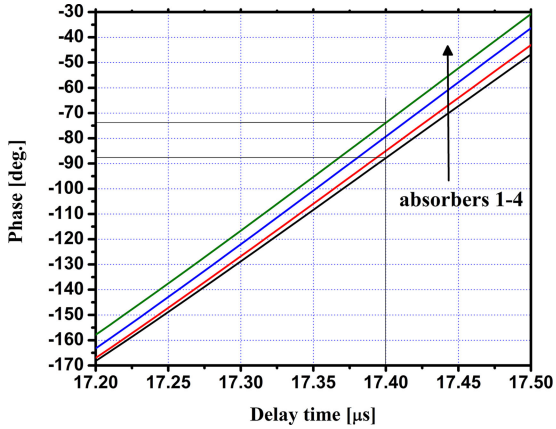

Fig. 6. Phase near the peak of the PA signal.

was used with sheep blood to measure PA signals at 680 and 805 nm.

Sterile heparinized sheep blood (CL2581-500H; ON, CA) was purchased from Cederlane. The blood was stored at a 4 °C temperature in the laboratory refrigerator and was used during the three-week expiration period. In order to ensure the homogeneity of the blood, the bottle was manually shaken well before use. Using a syringe, 60 ml of blood was transferred from the bottle to a 100-ml commercial blood bag (containing two standard size openings). Consequently, to create a vacuumed system, the air present in the blood bag was squeezed out. Upon concluding these preparations, the remaining parts of the *in-vitro* blood circulation system were assembled. The peristaltic pump was used to generate suction at one end of a tube while the other end was connected to one of the openings of the blood bag without introducing air into the system. An additional tube was used where one end was connected to the peristaltic pump while the other, pressurized end, was placed in a disposal flask. The sheep blood was allowed to circulate continuously at a speed of 12 r/min. After the circulating blood ejected all the air in the system, the pressurized end was connected to the second opening of the blood bag. The room temperature was kept at 20 °C at all times.

The circulating system was a closed system and therefore, blood hematocrit (hct) remained constant during the experiments. Blood oxygenation was reduced from ∼100% to less than 70% in several steps by adding a small amount of sodium dithionite (Na2O4S2; Sigma-Aldrich, MO, USA) in each step [34], [38]. Each time, a specific amount of the chemical powder was diluted in ∼1.5 ml of fresh sheep blood and the diluted solution was slowly injected into the circulation system using a syringe. In order to stabilize the oxygenation levels in the whole system, the blood was allowed to circulate for 20 min afterwards. A blood gas analyzer, (CCA-TS, OPTI Medical System, Inc, Roswell, GA, USA) was used to measure the oxygenation level independently. The employed blood gas analyzer uses the optical reflectance at three wavelengths of 670, 780 and 850 nm to calculate both tHb and SO_2, where the errors of these parameters are ±1.5 g/dl and ±2%, respectively [39]. In each step, approximately 0.3 ml of blood was extracted from the circulating system using a new syringe and was uploaded to a B-Cassette

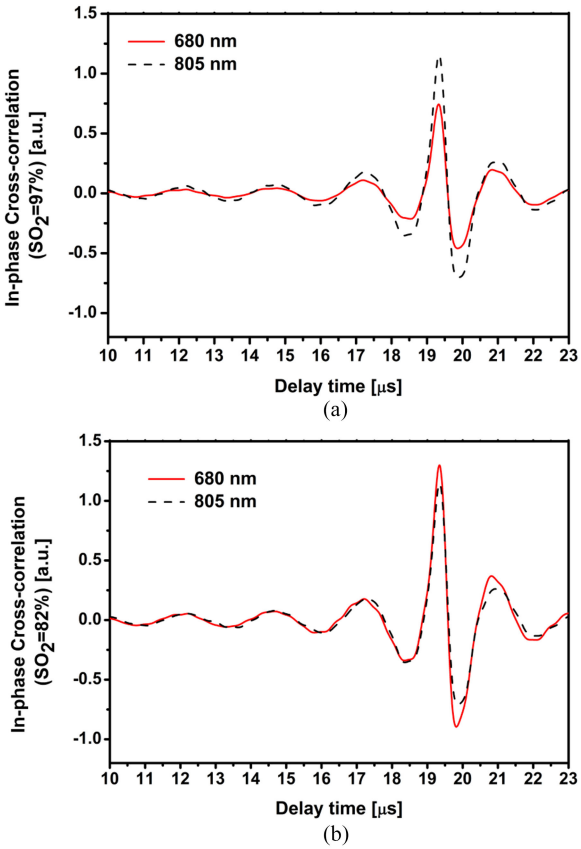

Fig. 7. In-phase PA CC signals with two wavelengths at (a) 97% and (b) 82% oxygenation.

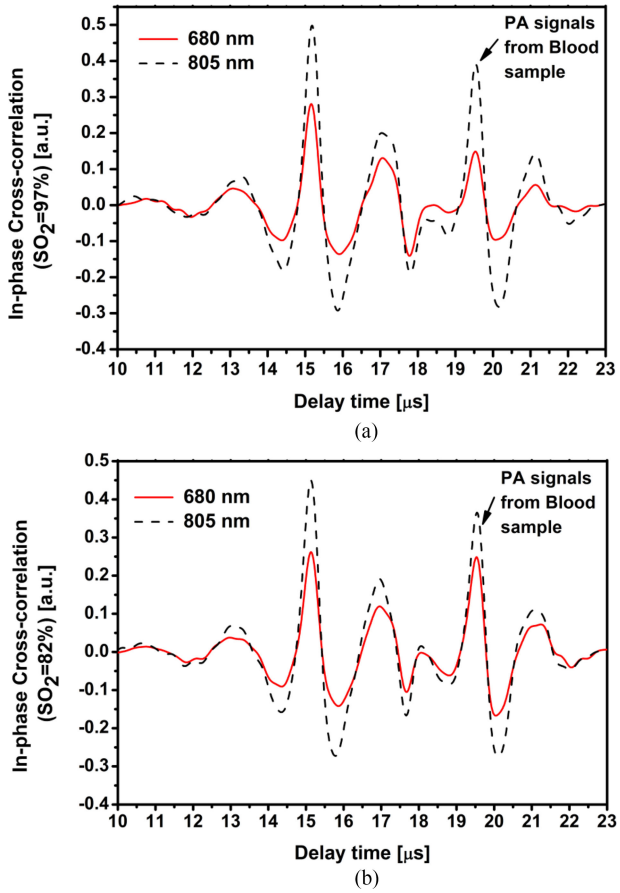

Fig. 8. In-phase PA CC signals with two wavelengths at (a) 97% and (b) 82% oxygenation when a 4-mm PVC-plastisol layer affects the laser emission.

(OPTImedical, GA, USA). The PA measurement on blood was performed in several steps with blood oxygenation level reduced in each step. This experiment was repeated four times, each time with new blood. The measurements of tHb using the gas analyzer for those four sets of experiments yield 11.7 ± 0.7 g/d1. This total hemoglobin concentration value is in the normal range for sheep blood reported in the literature [40], [41].

The PA measurements were performed by employing consecutive 1-ms frequency sweeps of 300 kHz to 2.5 MHz with 100-μs intervals between the excitation signals. The measurements were repeated 200 times for both wavelengths to provide the averaged detected signal. Therefore, the total laser exposure time for each measurement was 440 ms (with each laser emitting 200 ms of the 440 ms). This exposure time yields maximum permissible exposures (MPE) of 896 mJ/cm^2 and 1.45 J/cm^2 for 680 and 805 nm lasers, respectively [42]. Since the effect of laser light at these wavelengths is mainly thermal (on tissue), the fluence at each wavelength should be curbed to less than half of its calculated MPE. The total applied fluences of the 680 and 805 nm lasers for each measurement were 523 and 327 mJ/cm^2, respectively. The measurement at each blood oxygenation stage was repeated more than 10 times with $\sim$1 min interval between the measurements while the blood was circulating continuously. Signal averaging over these measurements helps reduce the effect of possible inhomogeneity in blood.

The PA CC signals for two measurements are shown in Fig. 7. Fig. 7(a) and (b) shows the in-phase CC of PA signals from two blood samples with 97% and 82% oxygenation levels, respectively. The ratio of the peak values at the two wavelengths can be employed to estimate SO_2.

During two sets of experiments, after PA measurements at each oxygenation level, a 4-mm plastisol layer attached to an aluminum frame was placed in front of the blood measurement cell. The optical absorption and scattering properties of the layer were completely distinct at wavelengths 680 and 805 nm and therefore, it was very difficult to calibrate the fluence that the circulating blood was exposed to. Fig. 8(a) and (b) corresponds to Fig. 7(a) and (b), respectively, when the interfering plastisol layer was placed in front of the measurement cell ($SO_2 = 97\%$ and 82%, respectively). The oxygenation level can be estimated using the conventional approach from the PA peak values. The PA estimates are compared to the SO_2 values determined by the gas analyzer and are shown in Fig. 9. When the illumination was not disturbed by the scattering overlayer, the SO_2 evaluated via PA amplitude and gas analyzer are very close, on average with a 1.6% difference. This error is in the range of the accuracy of the gas analyzer. It should be added that the values of SO_2 below 70% are out of the range of the gas analyzer, thus, the x-axis of cases below 70% (see Fig. 9) were only based on PA estimates. Another evidence of the accuracy of the PA signal is the variation of the 805 nm PA peak during the deoxygenation steps. 805 nm is approximately at the isosbestic point for sheep blood and as mentioned before, with the experimental set-up providing

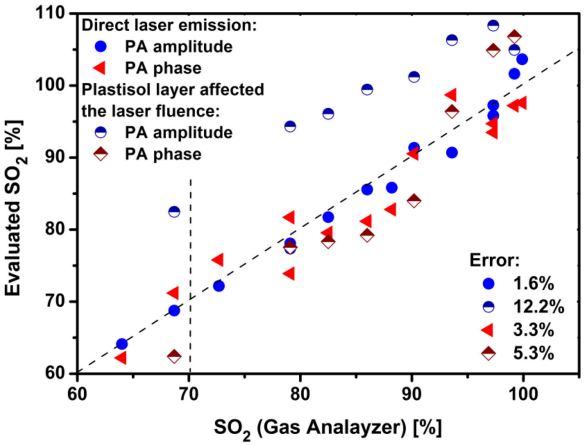

Fig. 9. SO_2 evaluated by PA amplitude and phase in both cases of direct laser emission and when the plastisol layer affects the fluence of both lasers.

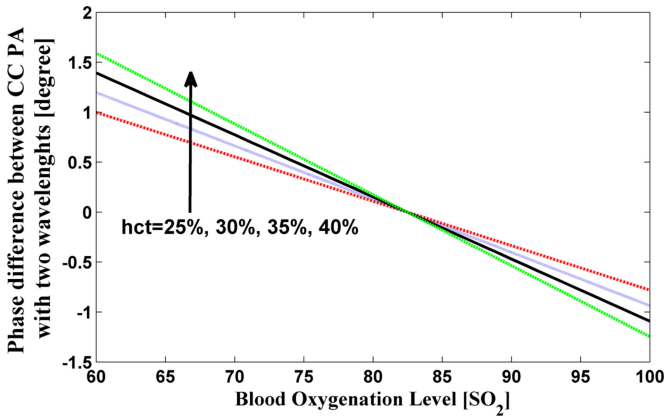

Fig. 10. Simulated phase difference between PA CC signals versus oxygenation level. The parameters of transducer, laser wavelengths and chirp bandwidth are identical to the experiment presented here.

a closed system, tHb was expected to remain constant. The variation of 805 nm PA peak in the four sets of measurements was only 4.4%.

When the plastisol layer was added to the set-up, the average error of the SO_2 estimations soared to 12.2%. While the geometry of this experiment was very simple, it demonstrated one of the main challenges of quantitative PA imaging. Having unknown absorption and scattering properties at the interrogated wavelengths, this layer makes it very difficult to calibrate the laser intensities reaching the target.

The same signal measurements were also used to calculate the SO_2 based on the difference in the phase around the peak of the PA signals measured with 680 and 805 nm laser irradiation, and using (11). The main advantage of (11) is that there is no need to find the $t - t_p$ value. The phase difference can be averaged around the signal peak. To correlate the phase difference with the oxygenation level, a simulation was performed using (3) where μ_a was estimated based on hct between 25% to 40% and SO_2 between 60% to 100%. The effect of the transfer function of the transducer is also included in the simulation. The results are shown in Fig. 10. Plots in Fig. 10 demonstrate that for each hct value, there is a linear relation between the phase difference and oxygenation level. It can be seen that all lines are intersecting at $SO_2 = 83\%$. This is due to the fact that the absorption coefficients of light for sheep blood at both 680 and 805 nm are similar at 83% oxygenation level. The phase differences of the detected signals were averaged around the peak, and used to evaluate SO_2. These SO_2 estimates are also shown in Fig. 9. It can be seen that the errors in SO_2 estimates with PA phase are larger than the peak value estimates in the simple experiments, 3.3% versus 1.6%. However, upon adding the plastisol layer, the phase estimation is shown to be much more robust. The error in SO_2 estimation by PA phase with the addition of the plastisol layer was 5.3% whereas the error for amplitude estimates in this case was 12.2%. This comparison shows that the phases of PA signals provide an advantage in quantitative PA imaging when fluence calibration is an issue.

VI. Discussion

It was shown that it is possible to obtain the absorption coefficient of a chromophore with the phase of the CC PA signal. The feasibility of the proposed method is demonstrated with experiments on PVC-plastisol samples. It was found that, although the distance from the chromophore and the speed of sound in the medium determine the location of the PA CC peak, other parameters such as absorption coefficient, limited bandwidth of the detector and acoustic attenuation also have a small effect on the peak location. The variation of the PA peak is normally so small that it has no effect on FD-PA generated images. However, using the phase of the PA signal for quantitative characterization requires evaluation of any peak shift. A fitting-based method was used to obtain the absorption coefficient of the samples. The estimated μ_a values from PA phase were compared with the μ_a values obtained from purely optical transmission as well as from the peak of the PA signal. Table I shows that the PA phase provides a more accurate estimate than the amplitude. However, it should be mentioned that the experiment was performed on an ideal sample. The phantoms were homogeneous, large-enough to be considered semi-infinite and had smooth and flat surfaces. Also, each measurement was performed on a sample with no other chromophore with spectral absorption nearby. This ideal situation was employed to experimentally validate the developed theory.

Furthermore, the difference in the phase of two PA signals at distinct wavelengths was used to estimate blood oxygenation level. Throughout the experiments, the estimated oxygenation levels were compared with the estimates from the conventional PA technique (using the signal amplitude) as well as with values determined by a commercial blood gas analyzer. The advantage of the PA phase spectroscopy method was demonstrated by adding one layer of plastisol material in front of the sample. Due to the difference in the absorption and scattering coefficients of this layer at the two employed wavelengths, large errors are generated in the oxygenation estimates based on the PA amplitude. However, the phase difference between the two signals exhibits less deviation and therefore, it provides higher accuracy in evaluating the SO_2.

The presented method is comparable with the PA risetime employed in pulsed PA [17], [18]. Both methods, the PA phase

and the pulsed PA temporal profile techniques were developed based on the 1-D PA solution. Among the most important limitations of using the temporal shape of the pulsed PA signal is the requirement for ultra-wideband detection. The major advantage of the present FD-PA phase spectroscopy technique is its capability to relax this limitation. The finite bandwidth is inherent in the theory and is controlled by the chirp frequency range. It should be mentioned that the present method is not restricted to FD-PA. Due to the similarity of the theory [43], it can be adapted for the pulsed PA signal as well.

The main limitation of the present method is that the geometry should be known and at this stage it is limited to a flat absorber. Future studies will focus on extending the experiments to cylindrical geometries, for example, plastic tubes filled with blood simulating human blood vessels. The exact PA solution for a 2-D cylindrical shape (finite cylinder) is already available [44]. For simplicity, a more simplified theory of 1-D cylindrical geometry (only radial direction) can be employed and can help extend the application of FD-PA spectroscopy to noninvasively determine blood oxygenation level in veins and arteries. It has been shown that the PA image can help determine the size of blood vessels [45], which, in turn, can help adjust the theoretically expected phase change expression based on the geometry.

To further extend the application of the proposed method to *in-vivo* functional imaging, besides geometry there are two other challenges. These obstacles are a) the high optical attenuation and b) the heterogeneity of the overlaying skin and tissue which reduce the light intensity and cause non-uniform fluence. These factors also affect the conventional deep PA imaging and spectroscopic methods. One suggested solution that may alleviate these effects is to irradiate the tissue from different directions [46], [47]. Laser irradiation from all accessible angles causes full tissue illumination and therefore, reduces the effect of tissue heterogeneity and enhances depth detectivity.

Before extending the experiments to the *in-vivo* stage, one intermediate step could be to wrap the abovementioned blood tube with chicken breast to simulate overlying tissue. Since the increase in laser fluence does not affect the phase values, to overcome the reduced SNR and depth detectivity, one may maximize SNR by driving the laser fluence to the maximum level and proportionally shortening the chirp time to remain below the safety limits. It was shown that reducing the laser exposure time tends to allow for a higher permissible laser fluence [48].

VII. Summary

It was theoretically shown that it is possible to obtain the absorption coefficient of a chromophore from the phase of the CC PA signal without knowledge of the actual laser fluence. The feasibility of the proposed method was demonstrated with experiments on PVC-plastisol samples. The method was also applied to evaluate the oxygenation level of *in-vitro* sheep blood. It was shown that PA phase spectroscopy is less sensitive to the absorption of laser light in the media surrounding the target absorber. The scattering and absorption properties of the surrounding material disturb the fluence inside a turbid medium, therefore affecting the PA amplitude in either time- or FD. On the other hand, the PA phase is not fluence dependent and therefore, does not require calibration. Phase measurements of the SO_2 were in error by 5.3% in the case of a turbid overlayer, whereas amplitude measurement error was 12.2%. The FD-PA phase spectroscopy method in single- or two-wavelength form can be used for accurate quantitative imaging of absorption coefficients in biological tissues without the need for laser fluence knowledge.

References

[1] A. Rosencwaig, "Photoacoustic spectroscopy of biological materials," *Science*, vol. 181, no. 4100, pp. 657–658, 1973.

[2] X. Wang *et al.*, "Noninvasive laser-induced photoacoustic tomography for structural and functional in vivo imaging of the brain," *Nature Biotechnol.*, vol. 21, pp. 803–806, 2003.

[3] S. Hu and L. V. Wang, "Photoacoustic imaging and characterization of the microvasculature," *J. Biomed. Opt.*, vol. 15, no. 1, pp. 011101-1–011101-15, 2010.

[4] P. Beard, "Biomedical photoacoustic imaging," *Interface Focus*, vol. 1, no. 4, pp. 602–631, 2011.

[5] X. Wang, X. Xie, G. Ku, L. V. Wang, and G. Stoica, "Noninvasive imaging of hemoglobin concentration and oxygenation in the rat brain using high-resolution photoacoustic tomography," *J. Biomed. Opt.*, vol. 11, no. 2, pp. 024015-1–024015-9, 2006.

[6] K. M. Stantz *et al.*, "Photoacoustic spectroscopic imaging of intra-tumor heterogeneity and molecular identification," *Proc. SPIE, Photons Plus Ultrasound, Imag. Sens.*, vol. 6086, pp. 8605-1–8605-5, 2006.

[7] S. Mallidi, G. P. Luke, and S. Emelianov, "Photoacoustic imaging in cancer detection, diagnosis, and treatment guidance," *Trends Biotechnol.*, vol. 29, no. 5, pp. 213–221, 2011.

[8] T. J. Allen, A. Hall, A. P. Dhillon, J. S. Owen, and P. C. Beard, "Spectroscopic photoacoustic imaging of lipid-rich plaques in the human aorta in the 740 to 1400 nm wavelength range," *J. Biomed. Opt.*, vol. 17, no. 6, pp. 061209-1–061209-10, 2012.

[9] A. Buehler, M. Kacprowicz, A. Taruttis, and V. Ntziachristos, "Real-time handheld multispectral optoacoustic imaging," *Opt. Lett.*, vol. 38, pp. 1404–1406, 2013.

[10] A. Needles *et al.*, "Development and initial application of a fully integrated photoacoustic micro-ultrasound system," *IEEE Trans. Ultrason. Ferroelectr. Freq. Control*, vol. 60, no. 5, pp. 888–897, May 2013.

[11] J. Laufer, D. Delpy, C. Elwell, and P. Beard, "Quantitative spacially resolved measurement of tissue chromophore concentrations using photoacoustic spectroscopy: Application to the measurement of blood oxygen and haemoglobin concentration," *Phys. Med. Biol.*, vol. 52, pp. 141–168, 2007.

[12] B. T. Cox, J. G. Laufer, and P. C. Beard, "The challenges for quantitative photoacoustic imaging," *Proc. SPIE*, vol. 7177, pp. 717713-1–717713-9, 2009.

[13] B. Cox, J. G. Laufer, S. R. Arridge, and P. C. Beard, "Quantitative spectroscopic photoacoustic imaging: A review," *J. Biomed. Opt.*, vol. 17, no. 6, pp. 061202-1–061202-22, 2012.

[14] M. Sivaramakrishnan, K. Maslov, H. F. Zhang, G. Stoica, and L. V. Wang, "Limitations of quantitative photoacoustic measurements of blood oxygenation in small vessels," *Phys. Med. Biol.*, vol. 52, pp. 1349–1361, 2007.

[15] A. A. Karabutov, N. B. Podymova, and V. S. Letokhov, "Time-resolved laser optoacoustic tomography of inhomogenous media," *Appl. Phys. B*, vol. 63, pp. 545–563, 1996.

[16] A. A. Karabutov, E. V. Savateeva, N. B. Podymova, and A. A. Oraevsky, "Backward mode detection of laser-induced wide-band ultrasonic transients with optoacoustic transducer," *J. Appl. Phys.*, vol. 87, no. 4, pp. 2003–2014, 2000.

[17] A. A. Oraevsky, S. L. Jacques, and F. K. Tittel, "Measurement of tissue optical properties by time-resolved detection of laser-induced transient stress," *Appl. Opt.*, vol. 36, no. 1, pp. 402–415, 1997.

[18] R. O. Esenaliev *et al.*, "Optoacoustic technique for noninvasive monitoring of blood oxygenation: A feasibility study," *Appl. Opt.*, vol. 41, no. 22, pp. 4722–4731, 2002.

[19] Y. Y. Petrov, I. Y. Petrova, I. A. Patrikeev, R. O. Esenaliev, and D. S. Prough, "Multiwavelength optoacoustic system for noninvasive monitoring of cerebral venous oxygenation: A pilot clinical test in the internal jugular vein," *Opt. Lett.*, vol. 31, no. 12, pp. 1827–1829, 2006.

[20] H. P. Brecht *et al.*, "In vivo monitoring of blood oxygenation in large veins with a triple-wavelength optoacoustic system," *Opt. Exp.*, vol. 15, no. 24, pp. 16261–16269, 2007.
[21] I. Y. Petrova *et al.*, "Noninvasive monitoring of cerebral blood oxygenation in ovine superior sagittal sinus with novel multi-wavelength optoacoustic system," *Opt. Exp.*, vol. 17, no. 9, pp. 7285–7294, 2009.
[22] I. Y. Petrov *et al.*, "Optoacoustic monitoring of cerebral venous blood oxygenation though intact scalp in large animals," *Opt. Exp.*, vol. 20, no. 4, pp. 4159–4167, 2012.
[23] Z. Guo, S. Hu, and L. V. Wang, "Calibration-free absolute quantification of optical absorption coefficients using acoustic spectra in 3D photoacoustic microscopy of biological tissue," *Opt. Lett.*, vol. 35, no. 12, pp. 2067–2069, 2010.
[24] Z. Guo, C. Favazza, A. Garcia-Uribe, and L. V. Wang, "Quantitative photoacoustic microscopy of optical absorption coefficients from acoustic spectra in the optical diffusive regime," *J. Biomed. Opt.*, vol. 17, no. 6, pp. 066011-1–066011-6, 2012.
[25] J. Xia *et al.*, "Calibration-free quantification of absolute oxygen saturation based on the dynamics of photoacoustic signals," *Opt. Lett.*, vol. 38, no. 15, pp. 2800–2803, 2013.
[26] J. Laufer, C. Elwell, D. Delpy, and P. Beard, "In vitro measurement of absolute blood oxygen saturation using pulsed near-infrared photoacoustic spectroscopy: Accuracy and resolution," *Phys. Med. Biol.*, vol. 50, pp. 4409–4428, 2005.
[27] Y. Wang and R. Wang, "Photoacoustic recovery of an absolute optical absorption coefficient with an exact solution of wave equation," *Phys. Med. Biol.*, vol. 53, pp. 6167–6177, 2008.
[28] G. M. Spirou, A. Mandelis, I. A Vitkin, and W. M. Whelan, "Frequency domain photothermoacoustic signal amplitude dependence on the optical properties of water: Turbid polyvinyl chloride-plastisol system," *Appl. Opt.*, vol. 47, no. 14, pp. 2564–2573, 2008.
[29] B. Lashkari, S. S. Choi, M. E. Khosroshahi, E. Dovlo, and A. Mandelis, "Simultaneous dual-wavelength photoacoustic radar imaging using waveform engineering with mismatched frequency modulated excitation," *Opt. Lett.*, vol. 40, no. 7, pp. 1145–1148, 2015.
[30] S. Choi *et al.*, "Wavelength-modulated differential photoacoustic spectroscopy (WM-DPAS): Theory of a high-sensitivity methodology for the detection of early-stage tumors in tissue," *Int. J. Thermophys.*, vol. 36, pp. 1305–1311, 2015.
[31] S. Choi *et al.*, "Wavelength-modulated differential photoacoustic spectroscopy (WM-DPAS) for noninvasive early cancer detection and tissue hypoxia monitoring," *J. Biophoton.*, to be published.
[32] B. Lashkari and A. Mandelis, "Linear frequency modulation photoacoustic radar: Optimal bandwidth for frequency-domain imaging of turbid media," *J. Acoust. Soc. Amer.*, vol. 130, no. 3, pp. 1313–1324, 2011.
[33] B. Lashkari and A. Mandelis, "Coregistered photoacoustic and ultrasonic signatures of early bone density variations," *J. Biomed. Opt.*, vol. 19, no. 3, pp. 036015-1–036015-11, 2014.
[34] W. G. Zijlstra, A. Buursma, and O. W. van Assendelft, *Visible and Near Infrared Absorption Spectra of Human and Animal Haemoglobin: Determination and Application*. Utrecht, the Netherlands: VSP, 2000.
[35] S. Prahl. (2015, Jul. 24). Optical absorption of hemoglobin [Online]. Available: http://omlc.ogi.edu/spectra/hemoglobin./
[36] N. Bosschaart, G. J. Edelman, M. C. G. Aalders, T. G. V. Leeuwen, and D. J. Faber, "A literature review and novel theoretical approach on the optical properties of whole blood," *Lasers Med. Sci.*, vol. 29, pp. 453–479, 2014.
[37] G. M. Spirou, A. A. Oraevsky, A. Vitkin, and W. M. Whelan, "Optical and acoustic properties at 1064 nm of polyvinyl chloride-plastisol for use as a tissue phantom in biomedical optoacoustics," *Phys. Med. Biol.*, vol. 50, pp. N141–N153, 2005.
[38] K. B. Sæbø and A. Bjørnerud, "Accurate de-oxygenation of ex vivo whole blood using sodium Dithionite," *Proc. Int. Soc. Magn. Reson. Med.*, vol. 8, p. 2025, 2000.
[39] OPTIMedical, "OPTI CCA-TS analyzer operator's manual," OPTI Medical Systems, Inc., Roswell, NM, USA, 2011.
[40] W. Allcroft, "Observations on the haemoglobin level of cows and sheeps," *J. Agric. Sci.*, vol. 31, no. 3, pp. 320–325, 1941.
[41] H. Holman, "Studies on the haemathology of sheep. I. The blood-picture of healthy sheep," *J. Comp. Pathol.*, vol. 54, pp. 26–40, 1944.
[42] "American national standard for the safe use of lasers," American National Standards Institute, Standard Z136.1-2007, New York, NY, USA, 2007.
[43] B. Lashkari and A. Mandelis, "Comparison between pulsed laser and frequency-domain photoacoustic modalities: Signal-to-noise ratio, contrast, resolution, and maximum depth detectivity," *Rev. Sci. Instrum.*, vol. 82, no. 9, pp. 094903-1–094903-14, 2011.
[44] J. Zalev and M. C. Kolios, "Exact solution for a photoacoustic wave from a finite-length cylindrical source," *J. Acoust. Soc. Amer.*, vol. 137, no. 4, pp. 1675–1682, 2015.
[45] R. G. M. Kolkman *et al.*, "Photoacoustic determination of blood vessel diameter," *Phys. Med. Biol.*, vol. 49, pp. 4745–4756, 2004.
[46] L. V. Wang and S. Hu, "Photoacoustic tomography: In vivo imaging from organelles to organs," *Science*, vol. 335, no. 6075, pp. 1458–1462, 2012.
[47] P. V. Es, S. K. Biswas, H. J. B. Moens, W. Steenbergen, and S. Manohar, "Initial results of finger imaging using photoacoustic computed tomography," *J. Biomed. Opt.*, vol. 19, no. 6, pp. 060501-1–060501-3, 2014.
[48] S. Telenkov and A. Mandelis, "Signal-to-noise analysis of biomedical photoacoustic measurements in time and frequency domains," *Rev. Sci. Instrum.*, vol. 81, no. 12, pp. 124901-1–124901-7, 2010.

Bahman Lashkari received the Ph.D. degree from the Center for Advanced Diffusion-Wave Technologies (CADIFT), University of Toronto, Toronto, ON, Canada, working on frequency-domain photoacoustic imaging in 2011. He is currently a Postdoctoral Research Associate at the CADIFT, where he works on several photoacoustic and ultrasound projects. His research interests include medical imaging and tissue characterization.

Sung soo Sean Choi received the B.Sc. degree in biomedical science from the University of Waterloo, Waterloo, ON, Canada, in 2012, and the M.A.Sc. degree in biomedical engineering from the University of Toronto, Toronto, ON, in 2015. His primary research interest includes developing a novel cancer diagnostic and monitoring applications using wavelength-modulated photoacoustic spectroscopy.

Edem Dovlo received the B.A.Sc. degree in mechanical engineering, the B.Sc. degree in computing technology, and the M.A.Sc. degree in mechanical engineering, all from the University of Ottawa, Ottawa, ON, Canada, in 2009, 2009, and 2011, respectively. She is currently working toward the Ph.D. degree at the Center for Advanced Diffusion-Wave Technologies, University of Toronto, Toronto, ON. Her research interests include improving early cancer diagnosis and care by using coregistered ultrasound and photoacoustic radar imaging systems.

Saheb Dhody is currently working toward the Undergraduate degree in mechanical engineering at the University of Toronto, Toronto, ON, Canada. Within his program, he is specializing in the fields of mechatronics and bioengineering. He is currently involved with the Center for Advanced Diffusion-Wave Technologies, Toronto, assisting with ongoing research in medical imaging.

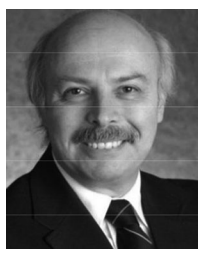

Andreas Mandelis is a Full Professor of mechanical and industrial engineering and electrical and computer engineering at the Institute of Biomaterials and Biomedical Engineering, University of Toronto, Toronto, ON, Canada. He is the Director of the Center for Advanced Diffusion-Wave Technologies, Toronto. He is an author and coauthor of more than 330 scientific papers in refereed journals and 180 scientific and technical proceedings papers. He is the Editor-in-Chief of the *International Journal of Thermophysics* and an Editor of the *Journal of Biomedical Optics*, the *Journal of Applied Physics*, and *Optics Letters*.